Multiple and Single Binding Modes of Fragment-Like Kinase Inhibitors Revealed by Molecular Modeling, Residue Type-Selective Protonation, and Nuclear Overhauser Effects

Keith L. Constantine,* Luciano Mueller, William J. Metzler, Patricia A. McDonnell, Gordon Todderud, Valentina Goldfarb, Yi Fan, John A. Newitt, Susan E. Kiefer, Mian Gao, David Tortolani, Wayne Vaccaro, and John Tokarski

Bristol Myers Squibb Research and Development, P.O. Box 4000, Princeton, New Jersey 08543

Received June 18, 2008

Fragment-like inhibitors of mitogen-activated protein kinase-activated protein kinase 2 (MK2) include 5-hydroxyisoquinoline ($IC_{50} \sim 85\ \mu M$). Modeling studies identified four possible binding modes for this compound. Two-dimensional $^1H-^1H$ NOESY data obtained with selectively protonated samples of MK2 in complex with 5-hydroxyisoquinoline demonstrated that two of the four predicted binding modes are well populated. A second small isoquinoline was subsequently shown to bind in a single mode. NMR and modeling studies using this general approach are expected to facilitate "scaffold hopping" and structure-guided elaborations of fragment-like kinase inhibitor cores.

Introduction

As key components of cellular signaling networks, kinases have become a major focus of small molecule drug discovery efforts.[1] Primary screens for kinase inhibitors are usually aimed at finding hits with K_d's (or IC_{50}'s) in the $1-10\ \mu M$ range, or better. The resulting hits, which often have characteristics that resemble those of drug-like or lead-like compounds,[2] are subsequently optimized to achieve the desired potency, selectivity, and efficacy.

Fragment-based approaches have been shown, in general, to be viable complements to other screening and lead-discovery strategies.[3] With regards to fragment-based screening applied to kinases, McCoy and co-workers have demonstrated that "novel kinase cores" can be identified by using STD[a]-based ATP-displacement assays.[4] They have also shown that qualitative structural information can be obtained by paramagnetic relaxation enhancement. The fragment-based interligand nuclear Overhauser effect approach has been used to discover novel inhibitors of p38α.[5] Recently, the progression from an initial "scaffold", a fragment-like compound ($IC_{50} > 200\ \mu M$) that displayed multiple binding modes, to a potent ($IC_{50} \sim 13$ nM), selective lead against an oncogenic mutant of B-Raf kinase was demonstrated.[6] This latter accomplishment included the determination of over 100 X-ray crystal structures of kinase−inhibitor complexes. In general, the progression from fragments to leads depends critically on the availability of structural data.[3]

Here, we demonstrate that detailed structural information on kinase−inhibitor complexes can be obtained by incorporating protonated (i.e., unlabeled) amino acids of one or more specific residue types into an otherwise highly deuterated kinase and then recording and analyzing 2D $^1H-^1H$ NOESY spectra of the kinase and kinase−inhibitor complexes.[7] This methodology is applicable both to potent, lead-like or drug-like inhibitors (Supporting Information), and to weak, fragment-like inhibitors. For fragments, we first demonstrate that multiple, discrete binding modes can be discerned from modeling studies combined with analysis of 2D NOESY data and that subsequent NMR and modeling studies of analogues can identify compounds that bind in a single (or highly dominant) mode. Our studies were performed with mitogen-activated protein kinase-activated protein kinase 2 (MK2).[8] In addition to weak inhibitors, we have used NMR to characterize the binding modes of relatively potent ($IC_{50} < 1\ \mu M$) MK2 inhibitors; an example is described in the Supporting Information.

Results and Discussion

MK2 samples were prepared with selectively protonated valine, leucine, methionine, threonine, lysine, and/or histidine residues. As described in detail in the Supporting Information, two MK2 constructs (constructs 1 and 2), both with autoinhibitory C-terminal residues removed, were used for the NMR studies. Construct 1 (with terminal truncations only) was used for earlier experiments. During the course of the project, construct 2 (with terminal truncations and an activation loop deletion) was produced. This construct, which has significantly improved thermal stability, was used for all subsequent NMR studies.

We have observed and assigned protein−inhibitor NOEs arising from the following residues in or near the ATP binding pocket: V78, K93, H108, V118, M138, and T206. Protein−inhibitor NOEs involving L70, L141, and/or L193 have also been observed and, in some cases, tentatively assigned. We note here that 2D $^1H-^1H$ NOESY spectra of apoprotein samples were routinely recorded prior to the addition of inhibitors in order to identify intraprotein NOEs, including any due to unexpected residual protonation. Before describing studies of MK2−inhibitor complexes, we first discuss how assignments for residues in the MK2 ATP binding site were obtained. Protein expression, NMR sample preparation, and NMR experimental details are described in the Experimental Section.

Residues in the MK2 ATP binding pocket that could potentially yield NOE interactions with inhibitors include three leucines (L70, L141, and L193), two valines (V78 and V118), one methionine (M138), one lysine (K93), one histidine (H108), and one threonine (T206). These residues are amenable to residue type-selective protonation. Resonances from M138, K93, H108, and T206 can be assigned by direct inspection in

* To whom correspondence should be addressed. Phone: 609-252-6926. Fax: 609-252-6012. E-mail: keith.constantine@bms.com.

[a] Abbreviations: C1, construct 1; C2, construct 2; HSQC, heteronuclear single quantum coherence; MK2, mitogen-activated protein kinase-activated protein kinase 2; MurB, the *Escherichia coli* MurB gene-encoded uridine diphosphate-*N*-acetylenolpyruvylglucosamine reductase; NOE, nuclear Overhauser effect; STD, saturation transfer difference; τ_m, mixing time.

10.1021/jm800747w CCC: $40.75
Published on Web 09/05/2008

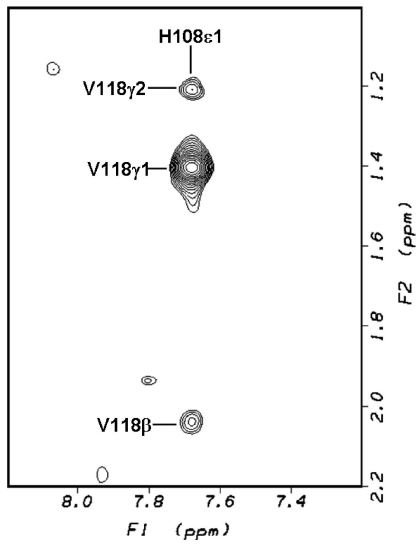

Figure 1. Region of a 2D ^{1}H−^{1}H NOESY spectrum (τ_m = 60 ms; protein concentration = 60 μM) of HV−^{2}H−MK2-C1 (apoprotein) showing NOE peaks between the side chains of V118 and H108.

MK2−inhibitor samples containing only the single corresponding residue type in protonated form, provided that protein−ligand NOEs are observed.

To obtain sequence-specific assignments for the two valine side chains, a sample of MK2 (construct 1) containing ^{1}H-His and ^{1}H-Val in a ^{2}H background (HV−^{2}H−MK2-C1) was prepared. On the basis of known X-ray structures of MK2 (e.g., protein data bank entries 1NXK and 1NY3), the only NOEs expected between histidine and valine side chains are between H108 and V118. Figure 1 shows a portion of a 2D ^{1}H−^{1}H NOESY spectrum recorded on apo-HV−^{2}H−MK2-C1. The observed NOEs allow assignments to be made for V118 Hβ (2.04 ppm), V118 γ1-methyl (1.41 ppm), V118 γ2-methyl (1.21 ppm), H108 Hε1 (7.68 ppm), and H108 Hδ2 (6.89 ppm). The V118 methyl resonances are stereospecifically assigned based on the distinct relative intensities of the NOEs between γ1- and γ2-methyl groups and H108 Hε1 (Figure 1) and the known MK2 X-ray structures. These methyl resonances are shifted significantly downfield relative to the average chemical shift positions for these atom types (http://www.bmrb.wisc.edu/ref_info/statsel.htm), as expected based on the relative orientations of V118, H108, and F208. (Hinge-binding aromatic moieties of inhibitors cause further downfield shifts for these resonances, as expected based on their orientations with respect to V118.) For ^{1}H-Val labeled MK2 samples, NOEs between inhibitors and V78 can be assigned by elimination. The three leucines have not been sequence-specifically assigned. Nevertheless, NOEs between the leucine residues and inhibitors can provide important information even without sequence-specific assignments.

Using construct 2, a fragment-based screen of MK2 was performed in the presence of an excess of a weak inhibitor (IC_{50} ~ 84 μM) known to bind to the ATP binding pocket (Supporting Information). Compounds that displaced the weak inhibitor were identified. The most potent fragment obtained from the screen was 5-hydroxyisoquinoline (Chart 1, compound **1**), which has an IC_{50} of ~85 μM.

The binding mode of **1** was investigated by molecular modeling and NMR. The modeling studies suggested four possible binding modes. Two of these binding modes have the hydroxyl of compound **1** accepting a H-bond from the backbone HN of L141 (the "hinge") and differ mainly by a ~180° rotation about an axis connecting the bridgehead carbons of **1**. A small

Chart 1. Fragment-Like MK2 Inhibitors (Isoquinolines)

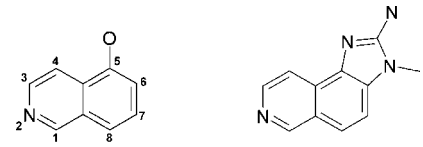

1 **2**

population of at least one of these modes is indicated by the NMR data, as described below. The remaining two predicted modes (designated A and B) both have N2 (standard isoquinoline numbering; see Chart 1) accepting a H-bond from L141 HN and differ mainly by a ~180° rotation about an axis connecting N2 and C5. Figure 2 shows models of binding modes A and B, in relation to the V78, V118, M138 side chains, and the backbone HN of L141.

A sample containing a 10-fold excess of compound **1** in the presence of MK2 showed significant broadening of H1 and (especially) H3 (Figure 3A), consistent with H-bonding of N2 to L141 HN (Supporting Information). Known structures of kinase−isoquinoline complexes[9] also show N2 H-bonding to the hinge, with the isoquinoline ring in the same overall orientation as predicted binding mode B of compound **1**. Our NMR data (described below) indicate that both modes A and B are significantly populated by compound **1**.

Two-dimensional ^{1}H−^{1}H NOESY spectra of MK2 in complex with compound **1** were collected using three different MK2 labeling schemes: ^{1}H-Met and ^{1}H-Val in a ^{2}H background (MV−^{2}H−MK2-C2), ^{1}H-His, and ^{1}H-Val in a ^{2}H background (HV−^{2}H−MK2-C2) and ^{1}H-Leu and ^{1}H-Thr in a ^{2}H background (LT−^{2}H−MK2-C2). (Chemical shift assignments and peak listings are in the Supporting Information.). Portions of spectra collected with HV−^{2}H−MK2-C2 and MV−^{2}H−MK2-C2 are shown in parts A and B of Figure 3, respectively. The data shown in Figure 3A were used to assign the inhibitor ^{1}H resonances (Supporting Information).

In Figure 3B, a very strong NOE peak between the M138 ε-methyl and the H4 proton of **1**, and additional strong-to-medium NOEs between H3 and V118, between H3 and M138, and between H4 and V118, are consistent with binding mode A (Figure 2A). However, NOEs observed between the H7 and H8 resonances of **1** and V118 and M138 are consistent with binding mode B (Figure 2B). In addition, weak NOEs between H6 and the V118 methyls, and between H1 and a V78 methyl, suggest that one or more low-population modes exist with hydroxyl of **1** H-bonded to the hinge. A strong NOE between H6 and a V78 methyl is consistent with a significant population of either mode A or B or of both (Figure 2). Overall, the results indicate a dynamic equilibrium between multiple modes. The simultaneous observation of NOEs from H1, H4, and H8 to the same leucine resonances (Figure S1, Supporting Information) is also consistent with a dynamic equilibrium between modes A and B (Figure S2, Supporting Information).

These results prompted a search for simple isoquinolines that, if active, may occupy only a single binding mode. A compound (Chart 1, compound **2**) was identified that occupies only binding mode A (shown modeled in Figure 4), as demonstrated by a 2D NOESY spectrum of this compound in complex with MV−^{2}H−MK2 (Figure 5). For compound **2** (2-amino-3-methyl-3*H*-imidazo[4,5-*F*]isoquinoline; IC_{50} ~ 15 μM), the most intense NOE observed is from H4 the M138 ε-methyl, and NOEs are also observed between H4 and V118, between H3 and V118, and between H4 and V118 (Figure 5C). There are no NOEs involving V118 and M138 with H1, H7, H8, or the methyl of

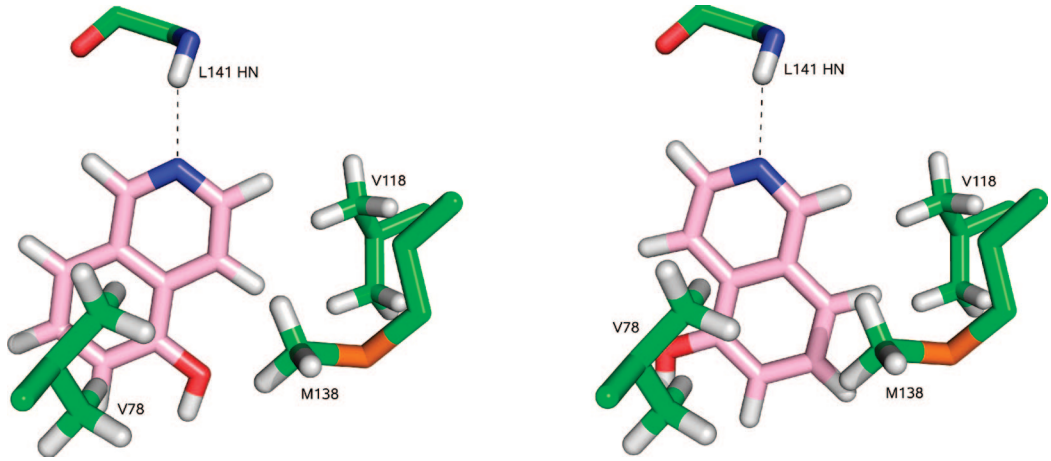

Figure 2. Two of the four predicted binding modes for compound **1** (carbons in pink) in complex with MK2. These two modes have N2 hydrogen-bonded to L141 HN. Predicted mode A is on the left and mode B is on the right. The main chain atoms of L141 are shown.

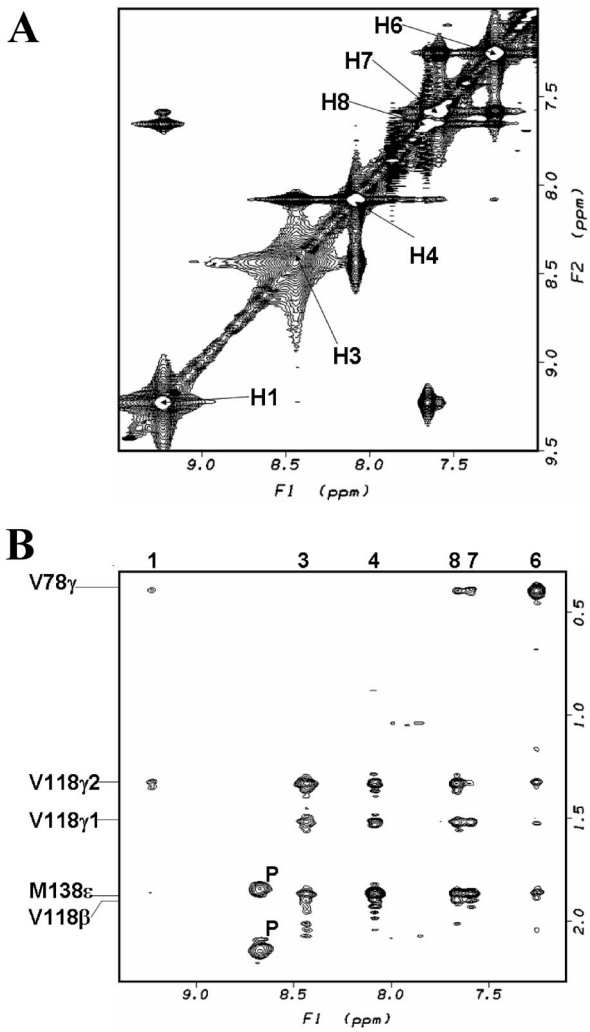

Figure 3. Regions of 2D $^{1}H-^{1}H$ NOESY spectra of MK2 in complex with compound **1**. (A) Aromatic region with **1** in complex with HV$-^{2}H-$MK2-C2 ($\tau_m = 30$ ms). Diagonal peaks and intraligand cross-peaks are shown. Diagonal peaks are labeled with their proton assignments. (B) Protein aliphatic-ligand aromatic region of **1** in complex with MV$-^{2}H-$MK2-C2 ($\tau_m = 60$ ms) showing protein−inhibitor NOEs and intraprotein peaks ("P"). The latter are due to unassigned, residual protonation of the protein in this sample. The MK2 and compound concentrations were 0.18 and 1.80 mM, respectively, for both samples.

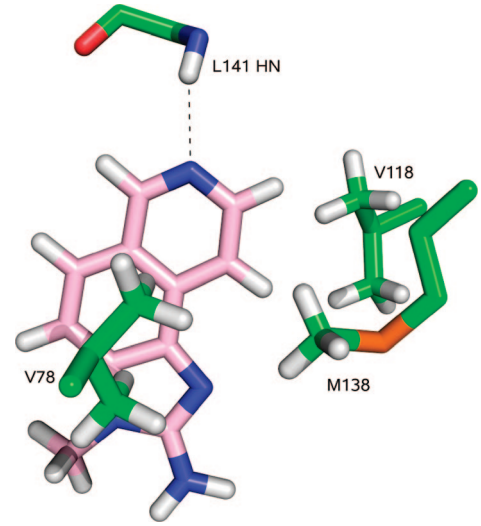

Figure 4. Modeled binding mode for compound **2** (carbons in pink) in complex with MK2 showing the Cα atoms and side chains of V118, M138, and V78 as well as the backbone atoms of L141.

compound **2**. These data indicate that only binding mode A is detectably populated for compound **2**. Given that mode B has been observed in other kinases for more extensively elaborated isoquinolines,[9] it is clear that either mode can be stabilized by appropriate placements of moieties on the isoquinoline ring.

Residue type-selective labeling is a widely applicable approach for observing protein−ligand NOEs in larger systems. Isotope-filtered NMR methods[10] can be used in conjunction with uniformly $^{13}C/^{15}N$-labeled proteins to observe protein−ligand NOEs. However, these methods suffer from severe sensitivity loss as rotational correlation times increase, limiting their application to relatively small proteins. We have measured a 3D ^{13}C-edited, $^{13}C/^{15}N$-filtered HSQC-NOESY spectrum on uniformly $^{13}C/^{15}N$-labeled MK2 (C2) in complex with a proprietary lead compound at 35 °C. While 20 protein−ligand NOEs were identified in this spectrum, the sensitivity was low relative to 2D $^{1}H-^{1}H$ NOESY data obtained at 15 °C using residue type-selective protonation. In addition to providing greatly enhanced sensitivity, residue type-selective labeling also directly provides information about the residue type(s) giving rise to protein−ligand NOEs. We have previously applied residue type-selective protonation of tyrosine residues to observe NOEs to $NADP^{+}$ in the MurB enzyme.[11] Taking advantage of the favorable relaxation properties of methyl groups, residue

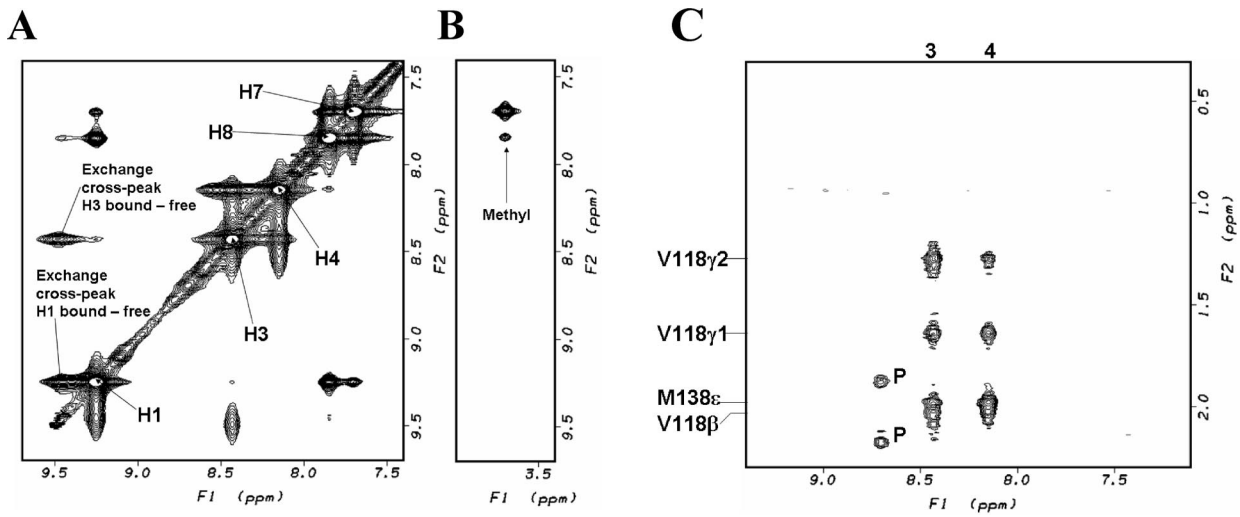

Figure 5. Regions of a 2D $^1H-^1H$ NOESY spectrum (τ_m = 60 ms) of MV−^2H−MK2-C2 in complex with compound **2**. (A) Aromatic region showing diagonal peaks and intraligand cross-peaks. (B) Aromatic−aliphatic region showing intraligand cross-peaks. (C) Protein aliphatic-ligand aromatic region showing protein−inhibitor NOEs and intraprotein peaks ("P") due to unassigned, residual protonation of the protein in this sample. The MK2 and compound concentrations were 0.18 and 1.80 mM, respectively.

type/atom type-selective $^1H/^{13}C$-labeling of methionine, isoleucine, and threonine residues has been used to observe NOEs in large (>100 kDa) enzyme−ligand complexes.[12]

Observing protein−ligand NOEs using residue type-selective labeling may prove difficult for proteins with highly polar binding sites, such as that of neuraminidase,[13] that contain relatively few methyl or aromatic side chains. Sparse protein−ligand NOE data must be used with caution. In the case of MK2, the hinge H-bond donor L141, and its immediate surroundings deep in the ATP pocket, appear to be relatively rigid based on comparisons of X-ray structures with different bound ligands. With a potent, elaborated proprietary lead compound, we observed NOE interactions between the inhibitor and the protein that could not be explained by an initial model of the complex. A subsequent X-ray structure demonstrated a large movement of the P-loop upon compound binding, explaining the NOE data. These results demonstrate the need to distinguish regions of the protein that are likely to be rigid versus those that are likely to be flexible, especially with larger, potent compounds that may interact with flexible regions. These considerations hold for both experimental protein structures and homology models.

If a sufficient number of protein−ligand NOEs can be observed and assigned, ligands can be accurately placed using NMR restraints.[14] For cases like that reported here (with relatively sparse NOE data sets and relatively simple compounds), the NOE data has been used as an independent check and verification of force field-based modeling without explicit NMR restraints. It is clear by inspection of the NOE data (Figure 3B) that **1** samples more than one binding mode; using explicit restraints, an ensemble average approach[15] would be required to satisfy this experimental data without distorting the protein and/or ligand structure. Force field-based modeling, without NMR restraints, combined with inspection of NOESY data allowed us to readily distinguish between single and multiple binding modes.

Conclusions

In summary, we have demonstrated that residue type-selective protonation and 2D $^1H-^1H$ NOESY data can provide detailed information on kinase−inhibitor interactions. NOE data obtained for more potent inhibitors of MK2 are consistent with known binding modes (Supporting Information). Modeling studies combined with NOESY data revealed both multiple and single binding modes for weak inhibitors. A previously unobserved kinase−isoquinoline binding mode (mode A) was confirmed. Molecular modeling and NMR verification of binding modes should facilitate the elaboration of kinase inhibitor cores because new scaffold hopping[16] and fragment optimization[17] possibilities may be suggested (Figure S5, Supporting Information).

Experimental Section

NMR Sample Preparation. To prepare NMR samples of MK2 construct 2, purified MK2 samples (Supporting Information) were concentrated and buffer exchanged using a Centricon YM10 membrane into 25 mM Na_2PO_4, pH 7.5, 200 mM NaCl, 5 mM d-DTT, 2 mM $MgCl_2$, 8% D_2O. The protein was concentrated at pH 7.5 and with 200 mM NaCl. Samples containing 25 mM Na_2PO_4, pD 7.1, 50 mM NaCl, 0.5 M D-glycine, 5 mM d-DTT, 0.001% NaN_3, 100% D_2O could be directly exchanged using centrifugation. Samples at lower pH and salt were dialyzed against three changes of buffer at 4 °C using 25 mM Na_2PO_4, pH-6.5, 5 mM d-DTT, 0.001% NaN_3, 8% D_2O, or 25 mM Na_2PO_4, pD 6.1, 5 mM d-DTT, 0.001% NaN_3, 100% D_2O. Each dialysis was performed for ~16 h in 100 mL of buffer. For samples containing construct 1, the final 100% D_2O buffer contained 25 mM d-MES, 200 mM NaCl, 5 mM d-DTT, 5 mM $MgCl_2$, at pD 6.8. For the samples used for the figure shown in the article, MK2 and inhibitor concentrations were 0.18 mM and 1.8 mM, respectively. Sample volumes were 320 μL in 4 mm Norell NMR tubes. Final protein concentrations were determined by the guanidine-HCl method using an extinction coefficient of 45930 and 41970 for construct 1 and 2, respectively. Compounds **1** and **2** were purchased from Aldrich and Toronto Research Chemicals, respectively, and used without further purification. Concentrated DMSO-d_6 stock solutions of the compounds were prepared and added directly to the MK2 NMR samples.

NMR Experimental Procedures. Two-dimensional $^1H-^1H$ NOESY spectra were recorded on a Varian INOVA 600 spectrometer equipped with a Varian 5 mm $^1H/^{13}C/^{15}N$ triple-resonance, triple-axis PFG cold probe. Spectral widths were set to 8000 and 11000 Hz in F1 and F2, respectively. The spectra were recorded at 15 °C for samples containing MK2 construct 1 and at 20 °C for samples containing MK2 construct 2. NOESY spectra for samples of compounds **1** and **2** with MK2 were recoded with 256 complex t_1 increments, and with 112 or 144 transients per increment. Transients were collected in an interleaved fashion, with 16 transients/block. The acquisition time used was 120 ms, followed by a 2.7 s recovery delay. Shifted sine-bell squared apodization was applied to both dimensions prior to Fourier transformation.

Zero-filling was applied to yield 2048 × 2048 frequency-domain spectral matrices. NOESY mixing times (τ_m) of 30 and 60 ms were used, as specified in the figure captions.

The NMR-based screen (Supporting Information) was performed on a Bruker Avance 700 MHz spectrometer equipped with a Bruker 5 mm $^1H/^{13}C/^{15}N$ triple-resonance, triple-axis PFG cold probe and with a sample changer. Saturation transfer difference (STD) spectra[18] were collected at 20 °C. On-resonance protein irradiation was centered at 0.7 ppm with a 1.0 ppm bandwidth, and off-resonance irradiation was set at −10.0 ppm with the same bandwidth. The protein saturation was performed with a train of Gaussian pulses for a total saturation time of 4.3 s. For both the on- and off-resonance spectra, 288 transients were collected in an interleaved fashion (48 transients/block). An acquisition time of 500 ms was used, and the recovery delay was 4.5 s. The spectral widths are 10965 Hz over 32K data points. Percent STD values were calculated based on peak heights.

Molecular Modeling Procedures. Compound **1** was docked in to X-ray structures of MK2 using the GLIDE software (Schrodinger L.L C., New York) and then energy-minimized for 5000 steps of conjugate gradient minimization using the OPLS-AA force field[19] combined with GBSA continuum model,[20] an implicit solvation model. Residues within 8 Å of the ligand were allowed to relax, and local minima were identified. On the basis of the consistency observed between binding mode A and the NMR data, compound **2** was simply placed manually in to the ATP binding site so that the isoquinoline ring overlapped well with that of compound **1** while avoiding any steric clashes.

Supporting Information Available: Additional NOESY data for compound **1**. Tables of NOE peak assignments for complexes involving compounds **1** and **2**. Description of a study of MK2 in complex with a potent inhibitor. Overlays of compound **1** (modes A and B) with a known MK2/inhibitor complex. Details on the MK2 constructs and the NMR-based screening. Amino acids used for expression of labeled MK2 samples. Details of the MK2 inhibition assay, protein expression, and protein purification for NMR samples. This material is available free of charge via the Internet at http://pubs.acs.org.

References

(1) (a) Cohen, P. Protein Kinases: The Major Drug Targets of the Twenty-First Century. *Nat. Rev. Drug Discovery* **2002**, *1*, 309–315. (b) Veith, M.; Sutherland, J. J.; Robertson, D. H.; Campbell, R. M. Kinomics: Characterizing the Therapeutically Validated Kinase Space. *Drug Discovery Today* **2005**, *10*, 839–846. (c) Karaman, M. W.; Herrgard, S.; Treiber, D. K.; Gallant, P.; Atteridge, C. E.; Campbell, B. T.; Chan, K. W.; Ciceri, P.; Davis, M. I.; Eden, P. T.; Faraoni, R.; Floyd, M.; Hunt, J. P.; Lockhart, D. J.; Milanov, Z. V.; Morrison, M. J.; Pallares, G.; Patel, H. K.; Pritchard, S.; Wodicka, L. M.; Zarrinkar, P. P. A Quantitative Analysis of Kinase Inhibitor Selectivity. *Nat. Biotechnol.* **2008**, *26*, 127–132.

(2) Oprea, T. I.; Davis, A. M.; Teague, S. J.; Leeson, P. D. Is There a Difference Between Leads and Drugs? A Historical Perspective. *J. Chem. Inf. Comput. Sci.* **2001**, *41*, 1308–1315.

(3) Hajduk, P. J.; Greer, J. A Decade of Fragment-Based Drug Design: Strategic Advances and Lessons Learned. *Nat. Rev. Drug Discovery* **2007**, *6*, 211–219.

(4) McCoy, M. A.; Senior, M. M.; Wyss, D. F. Screening of Protein Kinases by ATP-STD NMR Spectroscopy. *J. Am. Chem. Soc.* **2005**, *127*, 7978–7979.

(5) Chen, J.; Zhang, Z.; Stebbins, J. L.; Zhang, X.; Hoffman, R.; Moore, A.; Pellecchia, M. A Fragment-Based Approach for the Discovery of Isoform-Specific p38α Inhibitors. *ACS Chem. Biol.* **2007**, *2*, 329–336.

(6) Tsai, J.; Lee, J. T.; Wang, W.; Zhang, J.; Cho, H.; Mamo, S.; Bremer, R.; Gillette, S.; Kong, J.; Haass, N. K.; Sproesser, K.; Li, L.; Smalley, K. S. M.; Fong, D.; Zhu, Y.-L.; Marimuthu, A.; Nguyen, H.; Lam, B.; Liu, J.; Cheung, I.; Rice, J.; Suzuki, Y.; Luu, C.; Settachatgul, C.; Shellooe, R.; Cantwell, J.; Kim, S.-H.; Schlessinger, J.; Zhang, K. Y. J.; West, B. L.; Powell, B.; Habets, G.; Zhang, C.; Ibrahim, P. N.; Hirth, P.; Artis, D. R.; Herlyn, M.; Bollag, G. Discovery of a Selective Inhibitor of Oncogenic B-Raf Kinase with Potent Antimelanoma Activity. *Proc. Natl. Acad. Sci. U.S.A.* **2008**, *105*, 3041–3046.

(7) Mueller, L.; Kumar, N. V. Multidimensional NMR of Macromolecules. In *NMR Spectroscopy and its Application to Biomedical Research*; Sarkar, S. K. , Ed.; Elsevier Science B.V.: Amsterdam, 1996; Chapter 2.

(8) Gaestel, M. MAPKAP Kinase, MKs: Two's Company, Three's a Crowd. *Nat. Rev. Mol. Cell. Biol.* **2006**, *7*, 120–130.

(9) (a) Engh, R. A.; Girod, A.; Kinzel, V.; Huber, R.; Bossemeyer, D. Crystal Structures of the Catalytic Subunit of cAMP-Dependent Protein Kinase in Complex with Isoquinolinesulfonyl Protein Kinase Inhibitors H7, H8, and H89. Structural Implications for Selectivity. *J. Biol. Chem.* **1996**, *271*, 26157–26164. (b) Breitenlechner, C.; Gassel, M.; Hidaka, H.; Kinzel, V.; Huber, H.; Engh, R. A.; Bossemeyer, D. Protein Kinase A in Complex with Rho-Kinase Inhibitors Y-27632, Fasudil, and H-1152P: Structural Basis of Selectivity. *Structure* **2003**, *11*, 1595–1607. (c) Collins, I.; Caldwell, J.; Fonseca, T.; Donald, A.; Bavetsias, V.; Hunter, L.-J. K.; Garrett, M. D.; Rowlands, M. G.; Aherne, G. W.; Davies, T. G.; Berdini, V.; Woodhead, S. J.; Davis, D.; Seavers, L. C. A.; Wyatt, P. G.; Workman, P.; McDonald, E. Structure-Based Design of Isoquinoline-5-sulfonamide Inhibitors of Protein Kinase B. *Bioorg. Med. Chem.* **2006**, *14*, 1255–1273.

(10) Breeze, A. L. Isotope-Filtered NMR Methods for the Study of Biomolecular Structure and Interactions. *Prog. NMR Spectrosc.* **2000**, *36*, 323–372.

(11) Constantine, K. L.; Mueller, L.; Goldfarb, V.; Wittekind, M.; Metzler, W. J.; Yanchunas, J.; Robertson, J. G.; Malley, M. F.; Friedrichs, M. S.; Farmer, B. T., III. Characterization of $NADP^+$ Binding to Perdeuterated MurB: Backbone Atom NMR Assignments and Chemical Shift Changes. *J. Mol. Biol.* **1997**, *267*, 1223–1246.

(12) Pellecchia, M.; Meininger, D.; Dong, Q.; Chang, E.; Jack, R.; Sem, D. S. NMR-Based Structural Characterization of Large Protein−Ligand Interactions. *J. Biomol. NMR* **2002**, *22*, 165–173.

(13) Klumpp, K.; Graves, B. J. Optimization of Small Moleculae Drugs Binding to Highly Polar Target Sites: Lessons from the Discovery and Development of Neuraminidase Inhibitors. *Curr. Top. Med. Chem.* **2006**, *6*, 423–434.

(14) Constantine, K. L.; Davis, M. E.; Metzler, W. J.; Mueller, L.; Claus, B. L. Protein−Ligand NOE Matching: A High-Throughput Method for Binding Pose Evaluation That Does not Require Protein NMR Resonance Assignments. *J. Am. Chem. Soc.* **2006**, *128*, 7252–7263.

(15) Constantine, K. L.; Mueller, L.; Andersen, N. H.; Tong, H.; Wandler, C. F.; Friedrichs, M. S.; Bruccoleri, R. S. Structural and Dynamic Properties of a β-Hairpin-Forming Linear Peptide. 1. Modeling Using Ensemble-Averaged Constraints. *J. Am. Chem. Soc.* **1995**, *117*, 10841–10854.

(16) Zhao, H. Scaffold Selection and Scaffold Hopping in Lead Generation: A Medicinal Chemistry Perspective. *Drug Discovery Today* **2007**, *12*, 149–155.

(17) Rees, D. C.; Congreve, M.; Murray, C. W.; Carr, R. Fragment-Based Lead Discovery. *Nat. Rev. Drug Discovery* **2004**, *3*, 660–672.

(18) Mayer, M; Meyer, B. Characterization of Ligand Binding by Saturation Transfer Difference NMR Spectroscopy. *Angew. Chem., Int. Ed.* **1999**, *38*, 1784–1788.

(19) Kaminski, G. A.; Friesner, R. A.; Tirado-Rives, J.; Jorgensen, W. L. Evaluation and Reparameterization of the OPLS-AA Force Field for Proteins via Comparison with Accurate Quantum Chemical Calculations for Peptides. *J. Phys. Chem. B* **2001**, *105*, 6474.

(20) Yu, Z.; Jacobson, M. P.; Friesner, R. A. What Role do Surfaces Play in GB Models? A New Generation of Surface-Generalized Born Model Based on a Novel Gaussian Surface for Biomolecules. *J. Comput. Chem.* **2006**, *27*, 72–89.

JM800747W